# Spatially resolved soft X-ray spectrometry from single-image diffraction

M. PRAEGER[1]*, A. M. DE PAULA[1†], C. A. FROUD[2], E. T. F. ROGERS[2], S. L. STEBBINGS[1], W. S. BROCKLESBY[2], J. J. BAUMBERG[1], D. C. HANNA[2] AND J. G. FREY[3]

[1]School of Physics and Astronomy, University of Southampton, Southampton SO17 1BJ, UK
[2]Optoelectronics Research Centre, University of Southampton, Southampton SO17 1BJ, UK
[3]School of Chemistry, University of Southampton, Southampton SO17 1BJ, UK
[†]Present address: Departamento de Fisica-ICEx, Universidade Federal de Minas Gerais, Caixa Postal 702, Belo Horizonte-MG 30123-970, Brazil
*e-mail: mattp@soton.ac.uk

Published online: 4 February 2007; doi:10.1038/nphys516

**High-harmonic generation (HHG) offers better coherence[1], shorter pulse durations[2] and far greater accessibility than synchrotron sources[3]. These factors make HHG an increasingly important source of soft X-rays and an excellent resource in many emerging areas, for example, the time-resolved study of conformational changes in single biological molecules[4]. Here, we demonstrate a novel technique that enables us to reconstruct spectral information spatially across an X-ray beam. As only a single diffraction image is required per measurement, this technique is well suited to time-resolved studies. This technique is applicable to many types of X-ray source[3,5–7] and can be adapted for different spectral regions. Here, results are obtained using a capillary high-harmonic source[8], revealing detailed information that brings new insight into the physical processes occurring inside the source and enabling us to show the first measurement of radial variation of harmonic order in the emission from an HHG capillary.**

Capillary high-harmonic generation (HHG) has the potential to be a very efficient source of soft X-rays because it offers an extended interaction length between the laser and the generating medium[9]. However, this potential has not yet been realized[10] because the propagation[11,12] and phase-matching[13,14] processes inside the capillary are complex and not fully understood. The aim of this work is to gain further insight into these complex processes by studying the variation of spectral output spatially across an HHG beam.

The HHG beam used was generated by a chirped-pulse-amplified Ti:sapphire laser as it was guided along the length of an argon-filled capillary. The spectro-spatial information was obtained through analysis of the diffraction pattern created by a nickel wire mesh inserted into the X-ray beam (see the Methods section).

Figure 1 shows an example of the diffraction pattern recorded on the CCD (charge-coupled device) camera. The overall spatial intensity profile of the beam is visible, although here we are more concerned with the effect of the nickel mesh. The X-rays are clearly diffracted by the grid of apertures, and on close inspection it is possible to observe different patterns at different positions across the beam, as seen in the insets in Fig. 1. The observed spatial variations in the diffraction pattern are due to spatial inhomogeneities in the X-ray beam spectrum, as can be confirmed with a grazing-incidence spectrometer (see Supplementary Information, Figs S1 and S2).

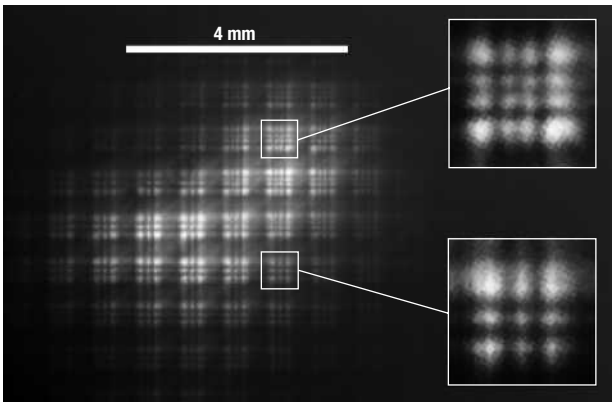


**Figure 1 Measured diffraction pattern for an argon pressure of 80 mbar.** The bar at the top of the image is 4 mm long in the plane of the CCD. The insets show regions of the measured diffraction pattern enlarged ×4 to clearly show the difference in the diffraction pattern at different locations across the X-ray beam. The integration time for this image was 100 ms.

The diffraction pattern observed is the coherent sum of all photons passing through the grid. With the typical experimental parameters used here however, light taking the direct path through an aperture to a point on the screen is at least three orders of magnitude more intense than light that has been diffracted via an adjacent aperture to arrive at the same point. This allows us to simplify the calculation considerably, by neglecting the effect of light from neighbouring apertures and considering the diffraction pattern created by each aperture separately. We have confirmed that this approximation is not the dominant source of error in our results.

The harmonic structure of our X-ray source enables us to make a further simplification; we neglect the spectral width of the harmonic peaks and calculate only the diffraction patterns due to

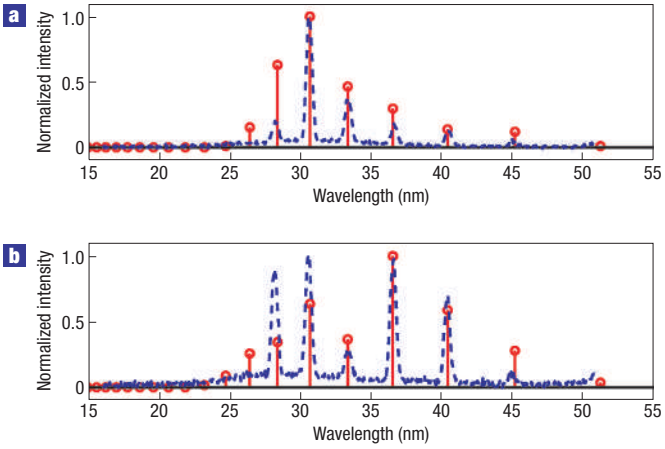


**Figure 2 High-harmonic X-ray spectra for argon in a capillary. a**,**b**, The spectrometer measured spectra (dashed line) and the reconstructed harmonic intensities (solid line) for argon pressures of 60 mbar (**a**) and 80 mbar (**b**). The integration time for the spectra was 20 s, the diffraction image used in the reconstruction was recorded in only 100 ms.

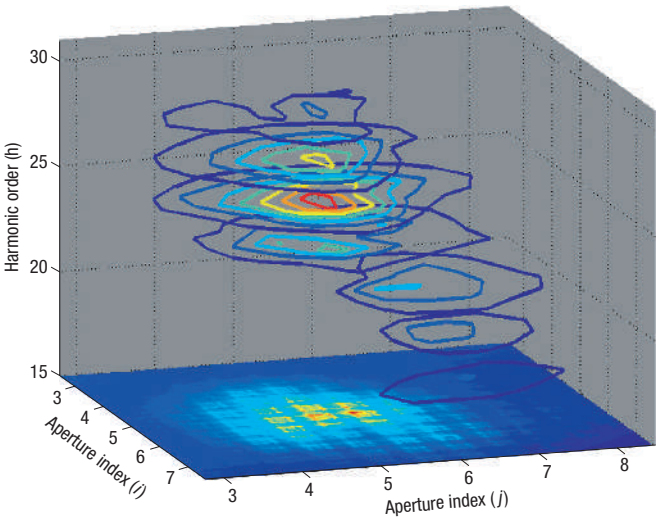


**Figure 3 An example of the spatially resolved reconstructed spectrum.** The pressure is set to 60 mbar and odd harmonics between the 17th and 31st orders are visible.

the centre wavelength of each harmonic order. Each diffraction pattern is calculated separately using standard Fresnel diffraction theory[15]. An incoherent sum may then be used to add these diffraction patterns (intensities rather than amplitudes) with a weighting factor proportional to the spectral intensity of each harmonic order (see the Methods section). The use of an incoherent sum to add the contributions from different harmonics is valid because the beat frequency between adjacent harmonics has a period of approximately 1 fs and interference between harmonics will therefore average out over the exposure time of the CCD.

A reconstructed X-ray spectrum is obtained by summing the harmonic-intensity coefficients of all of the apertures. The reconstructed spectrum for the whole beam is compared with the spectrum as measured using a grazing-incidence spectrometer. Note, however, that the spectrometer is only capable of sampling a thin slice of the beam with its slit. In addition, the diffraction and spectrometer measurements could not be recorded simultaneously. Nonetheless, there is an encouraging level of agreement between the measured and reconstructed X-ray spectra, see Fig. 2.

The reconstruction algorithm is not artificially weighted in any way and is free to allocate intensity into any odd harmonic of the laser up to the 51st; this limit is above the theoretical cutoff (imposed by the ionization potential of the gas and the ponderomotive potential of the laser) and can be arbitrarily extended simply by calculating more diffraction patterns. As can be seen in Fig. 2, the algorithm not only predicts intensity in the correct harmonic orders but the ratios of these intensities also show good agreement with the spectrometer data. This illustrates the power of our technique; although we are able to sample the entire beam with a single image in 100 ms, the spectrometer takes 60 s to integrate a single slice of the beam (see the Supplementary Information). Although the spectrometer can be translated across the X-ray beam, maintaining consistent alignment is challenging. In practice, the beam properties can substantially change while such an extended measurement is being made.

A further point to note about Fig. 2 is that the measured harmonic peaks do not correspond exactly to harmonics of the driving laser centre wavelength. We attribute this to blue-shifting of the input laser as it propagates through the capillary[8]. This blue-shift has been accurately modelled by considering the time variation of the apparent refractive index caused by changing the ionization fraction throughout the pulse. The highest harmonics are generated when the laser field is most intense near the centre of the capillary. This region of the capillary also has the highest ionization fraction at the time of emission and consequently the highest harmonics undergo a proportionally larger blue-shift. This blue-shifting is however a relatively subtle effect and we make no attempt to fit to it in the reconstruction.

The spectral reconstruction from a single diffraction image yields a wealth of information about the beam. We extract the two-dimensional (2D) spectral intensity (intensity versus harmonic order) as a function of spatial position across the beam. Figure 3 shows a visualization of this 4D spatio-spectral data as a stack of planes. On each plane is a 2D contour line plot showing the variation of spectral intensity in the two spatial dimensions. Each plane represents a different harmonic order, with the highest harmonics at the top. In this way, it is possible to show spectral intensity of each harmonic spatially across the beam. The base plane of the plot also shows the measured diffraction image. Visualizations such as this provide a very useful tool during data analysis.

This technique requires only a single image, thus it is possible to extract all of the spatio-spectral data from a single laser shot. (The images shown here were integrated over 100 laser shots in 100 ms to provide improved signal to noise.) The technique is therefore well suited to the study of transient properties of the HHG system or for eliminating shot-to-shot noise sources such as laser amplitude or carrier-envelope phase noise.

Figure 4 shows 2D plots of the data extracted from two diffraction images recorded at different pressures. The top row of the figure shows the spatial intensity distributions of the most intense harmonics generated with 60 mbar of argon in the HHG capillary. The data in the bottom row were extracted from the diffraction pattern recorded for 160 mbar of argon. Both sequences clearly show transverse spatial intensity profiles for each harmonic that are (approximately) cylindrically symmetric. The lower harmonic orders exhibit an annular intensity profile, whereas the higher energy harmonics occur as a spot whose

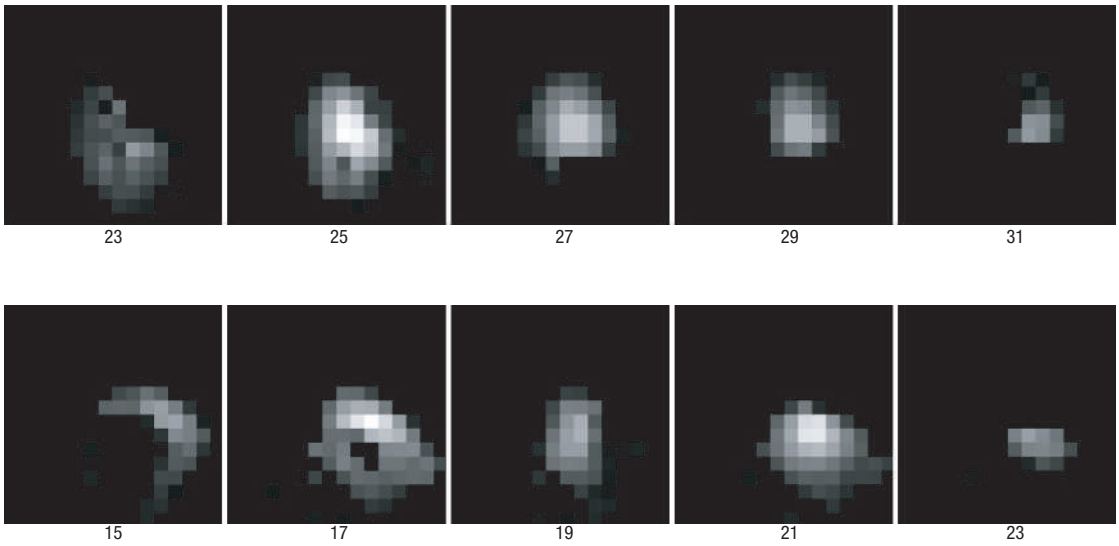


**Figure 4 Transverse spatial intensity profile as a function of harmonic order.** Two sequences are shown, each reconstructed from a single diffraction image. The argon pressure is 60 mbar (top row) and 160 mbar (bottom row). The numbers below the plots indicate the harmonic order.

radius decreases with increasing harmonic order. These intensity profiles are extremely sensitive to capillary alignment and pressure fluctuations. This is especially evident in the profiles at the lower left of Fig. 4 (15th and 17th harmonics at 160 mbar), where the intensity shifts to one side of the annulus.

Additional figures included in the Supplementary Information show the spatially resolved spectra as measured along the slit of our grazing-incidence spectrometer. These images show clear variation in the spectrum between different spatial positions and follow the same trends as observed in the sequences of Fig. 4.

The present work is the first to map the spatial and spectral profile of capillary-generated X-rays. This mapping gives information about the generation process that has until now been unavailable. The length over which X-rays are generated is limited both by the phase-matching coherence length and the absorption length in the generating gas. In argon, we are therefore limited to only a few millimetres of contributing path length even with perfect phase matching. Thus, X-rays are generated over a length less than the confocal parameter ($\sim$2 cm), meaning that spatial information about generation is not smeared out because of propagation effects. We therefore have a method that provides a quantitative measure of the spatial and spectral profile with which the X-rays are generated.

There are at least three possible mechanisms for the observed spatial variation of harmonics: radial changes in phase-matching conditions; non-collinear phase matching; or variation of the X-ray dipole phase with intensity giving a curved X-ray wavefront across the capillary[6]. As discussed below, the first of these generates collinear X-rays with a spatial variation, whereas the latter two generate X-rays with an angular distribution.

In capillary HHG, the factors affecting phase matching are neutral gas dispersion, plasma dispersion and waveguide dispersion. Previous work has shown low divergence for capillary-generated X-rays when they are phase matched, and high divergence when the phase-matching criteria are not met[9]. When high harmonics are generated in a gas, in general two possible electron trajectories contribute to each generated energy[16]. (Only one trajectory exists for X-rays generated at an energy close to cutoff.) These two trajectories are referred to as the long (where the electron takes approximately one optical cycle between tunnelling and recollision) and the short (in which the electron recollides after much less than one optical cycle) trajectories. In this experiment, as in most capillary generation, we are limited by phase matching to harmonics below the cutoff (which would be at the 49th harmonic in our case) and so both trajectories can contribute. For collinear phase matching, we assume a flat phase front for the generated X-rays, that is, the phase is locked to that of the driving laser and is not affected by the intensity of the fundamental. This is a good approximation for the short trajectories, but in the case of the long trajectories, the dipole phase is modified by the intensity of the driving laser leading to a curved wavefront and therefore an angular distribution of the generated X-rays. The long trajectories also have reduced coherence times compared with the short trajectories, so those X-rays that diverge most may exhibit less temporal coherence than the central beam[17]. Further experiments will be required to determine which mechanism produces the spatial variation in the X-ray spectrum observed in this experiment; however, this technique provides valuable new information with which to understand the variation.

The spatial resolution of this technique could be improved significantly by using a much finer pitched grid, as currently the aperture size is significantly greater than the shortest X-ray wavelengths we wish to probe (optimizing the diffraction grid design and the source-to-grid and grid-to-camera separations is the subject of further work). The reconstruction algorithm discussed in the Methods section makes use of prior knowledge that the output of an HHG soft X-ray source is composed of discrete spectral peaks at known wavelengths; this constrains the fit allowing a more robust reconstruction. Similar constrained algorithms could be produced for other types of source, however we are currently developing a more general algorithm that can be applied to a variety of sources without the need for *a priori* knowledge. In this experiment, we have demonstrated that spatially resolved spectral information can be recovered both rapidly and accurately from Fresnel diffraction patterns. We believe that this technique could be adapted for application in many other areas, however, in the case of HHG, these measurements provide vital experimental input into the testing of 3D phase-matching models and yield new insight into the physical processes of capillary HHG.

## METHODS

A Ti:sapphire chirped-pulse amplifier operating at 1 kHz is used to produce 1 mJ, 30 fs pulses centred at approximately 780 nm. These pulses are focused into a fused silica capillary of 75 μm bore radius which is 7 cm long but has a central active region 3 cm in length defined by two micromachined holes drilled through the side of the capillary. The ends of the capillary and the subsequent beam path are held under vacuum ($\sim 10^{-6}$ mbar) while argon gas is allowed to flow through the holes and into the active region at a controlled pressure. With this set-up, we observe generation of the odd harmonics, collinear with the driving laser field, up to the 31st harmonic at approximately 50 eV. A thin (200 nm) aluminium foil is used as a filter that transmits in the soft X-ray region but attenuates very strongly the infrared and visible light. (A useful source of X-ray transmission data is the Lawrence Berkeley National Laboratory Centre for X-Ray Optics website, which can be found at http://www-cxro.lbl.gov/.) In this experiment, a nickel wire mesh was used as a diffraction grating. This Ni grid is manufactured to high precision using electro-deposition through a lithographic resist mask, and consists of 38-μm-thick bars crossing perpendicularly to define an array of 335 μm square apertures (measured error in aperture size is $\sim 1\%$). The mesh is inserted into the beam 50 cm after the end of the capillary and the diffraction pattern this produces is recorded on an X-ray CCD camera positioned a further 1 m downstream.

For the diffraction pattern calculation, we use an incoherent sum to add the diffraction patterns of each single aperture with a weighting factor proportional to the spectral intensity of each harmonic order, $h$, in the $(i,j)$th aperture.

$$P_m(x,y,i,j) = \sum_{h=1}^{\infty} P_c(x,y,i,j,h) I(i,j,h). \qquad (1)$$

Here $x$ and $y$ are the spatial coordinates within the $(i,j)$th aperture and $h$ is an odd integer, as only odd harmonics are generated. If we begin with knowledge of the measured diffraction pattern due to one particular aperture $P_m(x,y,i,j)$, it is possible to use linear algebra to determine the set of harmonic intensity weighting coefficients $I(i,j,h)$ that produce the best fit between the measured data and the calculated data $P_c(x,y,i,j,h)$. The set of weighting coefficients $I(i,j,h)$ for any individual aperture $(i,j)$ and all harmonics $h$ give the reconstructed harmonic-peak spectral intensities. We used standard non-negative least-squares constraints to fit equation (1) to our measured diffraction patterns[18].

In practice, it is necessary to symmetrize the measured diffraction pattern of each aperture $P_m(x,y,i,j)$ before applying the fitting algorithm, thus eliminating the effect of small intensity gradients across the aperture. Each pattern is symmetrized by averaging the original image with its reflected counterparts in both axes. A background subtraction is also carried out.

The spatial resolution of this technique is most strongly dependent on the number of apertures illuminated by the beam. The spectral resolution is determined by the number of diffraction patterns (in the desired wavelength range) that can be uniquely distinguished by the CCD pixels. Inevitably there is a trade off to be made between these two factors. For a given aperture size and given source and CCD separations from the aperture, resolution is improved by moving to shorter wavelengths and larger beam diameters (provided that the interference fringes can still be resolved on the CCD pixels). However, the aperture size and the distances from the source and CCD to the aperture can be scaled to extend the validity of our approximations to quite a broad range of wavelengths while still remaining within the bounds of practicality.

Received 2 August 2006; accepted 19 December 2006; published 4 February 2007.

## References


1. Bartels, R. A. *et al.* Generation of spatially coherent light at extreme ultraviolet wavelengths. *Science* **297**, 376–378 (2002).
2. Hentschel, M. *et al.* Attosecond metrology. *Nature* **414**, 509–513 (2001).
3. Cavalieri, A. L. *et al.* Clocking femtosecond x rays. *Phys. Rev. Lett.* **94**, 114801 (2005).
4. Neutze, R., Wouts, R., van der Spoel, D., Weckert, E. & Hajdu, J. Potential for biomolecular imaging with femtosecond X-ray pulses. *Nature* **406**, 752–757 (2000).
5. Tamaki, Y., Itatani, J., Nagata, Y., Obara, M. & Midorikawa, K. Highly efficient, phase-matched high-harmonic generation by a self-guided laser beam. *Phys. Rev. Lett.* **82**, 1422–1425 (1999).
6. Salieres, P., L'Huillier, A. & Lewenstein, M. Coherence control of high-order harmonics. *Phys. Rev. Lett.* **74**, 3776–3779 (1995).
7. Dromey, B. *et al.* High harmonic generation in the relativistic limit. *Nature Phys.* **2**, 452–455 (2006).
8. Froud, C. A. *et al.* Soft-x-ray wavelength shift induced by ionization effects in a capillary. *Opt. Lett.* **31**, 374–376 (2006).
9. Rundquist, A. *et al.* Phase-matched generation of coherent soft x-rays. *Science* **280**, 1412–1415 (1998).
10. Christov, I. P. Enhanced generation of attosecond pulses in dispersion-controlled hollow-core fiber. *Phys. Rev. A* **60**, 3244–3250 (1999).
11. Pfeifer, T. *et al.* Spatial control of high-harmonic generation in hollow fibers. *Opt. Lett.* **30**, 1497–1499 (2005).
12. Wagner, N. L. *et al.* Self-compression of ultrashort pulses through ionization-induced spatiotemporal reshaping. *Phys. Rev. Lett.* **93**, 173902 (2004).
13. Durfee, C. G. *et al.* Phase matching of high-order harmonics in hollow waveguides. *Phys. Rev. Lett.* **83**, 2187–2190 (1999).
14. Paul, A. *et al.* Phase-matching techniques for coherent soft x-ray generation. *IEEE J. Quantum Electron.* **42**, 14–26 (2006).
15. Born, M. & Wolf, E. *Principles of Optics, Theory of Propagation, Iterference and Diffraction of Light* 7th edn (Cambridge Univ. Press, Cambridge, 1999).
16. Lewenstein, M., Salieres, P. & L'Huillier, A. Phase of the atomic polarization in high-order harmonic-generation. *Phys. Rev. A* **52**, 4747–4754 (1995).
17. Bellini, M. *et al.* Temporal coherence of ultrashort high-order harmonic pulses. *Phys. Rev. Lett.* **81**, 297–300 (1998).
18. Lawson, C. L. & Hanson, R. *Solving Least Squares Problems* Ch. 23, 161 (Prentice-Hall, New Jersey, 1974).


## Acknowledgements

This work was supported by the UK Research Councils through the Basic Technology Programme. Correspondence and requests for materials should be addressed to M.P. Supplementary Information accompanies this paper on www.nature.com/naturephysics.

## Author contributions

Experimental work: M.P., A.M.dP., C.A.F., S.L.S. Data analysis: M.P., E.T.R., W.S.B., J.J.B. Writing: M.P., A.M.dP., C.A.F., E.T.R., S.L.S., W.S.B., J.J.B., D.C.H., J.G.F. Project planning: W.S.B., J.J.B., D.C.H., J.G.F.

## Competing financial interests

The authors declare that they have no competing financial interests.